Preparation and Rheological Characterization of Intercalated Polystyrene/Organophilic Montmorillonite Nanocomposite

Tae H. Kim,[1] Sung T. Lim,[1] Chung H. Lee,[1] Hyoung J. Choi,[1] Myung S. Jhon[2]

[1]*Department of Polymer Science and Engineering, Inha University, Incheon, 402-751, Korea*
[2]*Department of Chemical Engineering, Carnegie Mellon University, Pittsburgh, Pennsylvania 15213-3890*

Received 8 November 2001; accepted 3 May 2002

ABSTRACT: Polystyrene (PS)/organophilic montmorillonite (OMMT) clay nanocomposites were prepared by a solvent casting method using chloroform as a cosolvent. Intercalation of the OMMT in the PS matrix was achieved as revealed by X-ray diffraction. The IR spectra of the products indicated that the OMMT is homogeneously dispersed in the PS matrix. A thermogravimetric analysis (TGA) showed that the onset temperature increases linearly with the clay content. The glass-transition temperature of the PS, examined using differential scanning calorimetry, had a trend similar to that from the TGA. The rheological properties of the PS/OMMT nanocomposites were also investigated via a rotational rheometer with a parallel plate geometry, and they exhibited sharper shear thinning and increased storage and loss modulus with clay content. Furthermore, the shear viscosity obtained from the steady shear experiment was well correlated with the complex viscosity obtained from the oscillatory experiment via the Cox and Merz relation. © 2003 Wiley Periodicals, Inc. J Appl Polym Sci 87: 2106–2112, 2003

Key words: rheology; polystyrene; clay; nanocomposite; viscoelastic property; montmorillonite

INTRODUCTION

Polymer/clay nanocomposites have attracted strong interest in recent materials research because they show substantial enhancements of material properties compared to the pristine polymers. These enhancements could be achieved even at low clay loadings. The mechanical and thermal improvements of small amounts of nanolayered clay (typically less than 10 wt %) are comparable with 30–50% loading of micron-sized fillers.[1] Further, compared to the prinstine polymers, polymer/clay nanocomposites possess many desirable properties including enhanced barrier characteristics,[2] increased modulus and strength,[3–6] a high heat distortion temperature,[7] a decreased thermal expansion coefficient,[2,8] reduced gas permeability,[9] a decrease in organic liquid absorption,[10] and enhanced ionic conductivity.[11–16] Recently, polymer/clay nanocomposites have been investigated as a potential material for electrorheological (ER) fluids.[17–20] A typical ER fluid consists of a suspension of micron-sized particles that exhibit drastic and reversible changes in their rheological properties when an external electric field is applied[21–23] in a nonconducting fluid. These improved properties depend on the nanostructured configuration and interfacial bonding between the clay and the polymer.[24]

Two morphologies of polymer/clay nanocomposites have been widely studied: intercalated structures and exfoliated structures. The intercalated nanocomposites are analogous to traditional inclusion or guest-host compounds, which result from polymer penetration into the interlayer and subsequent expansion to a thermodynamically stable spacing. The expansion of the interlayer is finite, typically on the order of 1–4 nm, and is normally associated with the incorporation of individual polymer chains. In contrast to intercalated composites, exfoliated nanocomposites consist of nanometer-thick silicate layers suspended in a polymer matrix, which result from extensive penetration of the polymer within and delamination of the crystallites. More significant property enhancements are observed for the exfoliated nanocomposites. These two nanocomposites are thought to be thermodynamically stable and have been predicted by mean field[25] and self-consistent[26] theories.

Intercalated and exfoliated polystyrene (PS)/clay nanocomposites have been widely investigated since Friedlander and Grink[27] observed a slight expansion of the d_{001} spacing of clay galleries upon intercalation. The melt intercalation of PS into organically modified sodium bentonite, a layered mica-type silicate, which leads to an approximate 25% increase in spacing between silicate layers, was also observed.[28] Further-

Correspondence to: H. J. Choi (hjchoi@inha.ac.kr).
Contract grant sponsor: Korea Science and Engineering Foundation (to Applied Rheology Center).

more, Hoffmann et al.[29] reported a correlation between the morphology and rheology of exfoliated PS/clay nanocomposites based on organophilic layered silicates such as fluoromicas. The intercalated PS/clay nanocomposites were prepared by polymerization of styrene in the organophilic and hydrophilic clays,[30] and this showed that the PS/clay nanocomposites exhibited better thermal stability than PS. Recently Chen et al.[31] reported Fourier transform IR (FTIR) spectra, thermal properties, and dispersibility of exfoliated PS/montmorillonite (MMT) nanocomposites.

In our study the PS/organophilic MMT (OMMT) nanocomposites were intercalated after the PS was dissolved with the OMMT in the suspension, followed by subsequent removal of the solvent. This solvent casting method has been adopted to produce various nanocomposite systems including poly(L-lactide)/MMT,[32] poly(ϵ-caprolactone)/MMT,[33] poly(vinyl alcohol)/Na^+-MMT,[1,34] and poly(ethylene oxide)/MMT[34,35] nanocomposites using either water or chloroform as a cosolvent. Moreover, to study the effect of clay loading, we prepared PS/OMMT nanocomposites with various clay contents and examined the microstructural and rheological properties for the PS/clay nanocomposites with increasing clay content.

EXPERIMENTAL

Materials

The OMMT (Cloisite 25A, Southern Clay Products Inc.) used in this study was an MMT modified by a cation exchange reaction with a dimethyl, hydrogenated tallow, 2-ethylhexyl, quaternary ammonium methylsulfate. The OMMT clays possess the same structural characteristics as the well-known minerals talc and mica (2:1 phyllosilicate) and comprise hydrated aluminum silicate.[36,37] However, the smectite clays are distinguished from talc and mica by a unit cell layer charge (typically, in the range of -0.6 to $-1.4/O_{20}$ unit) that is intermediate between the layer charge of talc ($0.0/O_{20}$ unit) and mica ($-2.0/O_{20}$ unit). This intermediate value for the layer charge leads to cation exchange and gallery swelling properties that are not shared by talc and mica.[38] The crystal structure of OMMT consists of 2-dimensional layers formed by fusing two silica tetrahedral sheets with an edge-shared octahedral sheet of either alumina or magnesia that exhibits a net negative charge on the lamellar surface, which enables them to adsorb cations such as Na^+ or Ca^{++}. Because these cations are not structural, they can be easily replaced by modifying the silicates with alkylammonium or phosphonium cations via an ion exchange reaction.[39,40] Depending on the functionality, packing density, and length of the organic modifiers, the OMMT may be engineered to optimize their compatibility with a given polymer.[41] The OMMT is a fine powder with an average particle diameter of 13 μm in the dry state with a cationic exchange capacity of 0.95 mEq/g and an ability to disperse well in chloroform. The PS (M_w = 230,000 g/mol) was purchased from Aldrich Chemical Co.

Preparation of nanocomposites

Both the PS and OMMT were dried in a vaccum oven at 25°C to remove moisture. A given amount (0.6, 1.5, or 3 g) of OMMT was dispersed in 200 mL of chloroform over 1 day at 25°C, and the matrix PS (29.4, 28.5, or 27 g) was also dissolved using the same method. The OMMT dispersions and PS solutions were mixed together by stirring for 2 days, and the mixtures were placed in glass dishes. After the chloroform was evaporated in a hood, all of the samples were subsequently dried in a vaccum oven for 2 days at 30°C. The weight percentage of OMMT in the nanocomposites is represented by the polymers; for example, PSOMMT10 indicates PS/OMMT nanocomposites containing 10 wt % OMMT.

Characterization

The insertion of the PS into the layers was confirmed with an X-ray diffraction (XRD) method. XRD diffractograms, were recorded by monitoring the diffraction angle 2θ from 1.5° to 30° on a Philips PW-1847 X-ray crystallographic unit monitored with a Guinier focusing camera. This unit was equipped with a nickel-filtered Cu K_α radiation source operated at 40 kV and 40 mA. The FTIR spectra for the OMMT, PS, and PSOMMT10 were recorded on a spectrum 2000 explorer spectrometer (Perkin–Elmer) in a range of 4000–450 cm^{-1} using a KBr pellet.

The thermal properties were also measured by thermogravimetric analysis (TGA, TGA 1000, Polymer Laboratories, Thermal Sciences Division). Samples of 10 mg were heated from 30 to 600°C at a heating rate of 20°C/min under a nitrogen environment. The thermal behavior of the nanocomposites was observed by differential scanning calorimetry (DSC, series 7, Perkin–Elmer). A sample of 5-mg mass was heated in a nitrogen atmosphere from 30 to 150°C with a heating rate of 10°C/min.

The rheological properties of the nanocomposites were investigated via a rotational rheometer (MCR 300, Physica) in a steady shear mode. Samples with 1-mm thickness and 25-mm radii were applied in a parallel plate geometry at a constant temperature of 200°C. The shear viscosity in the molten state sample was measured as a function of the shear rate. In addition, the rheological properties were investigated in an oscillatory shear experiment to measure the durability of the nanocomposites under vibration or periodic external stress. The experiment was carried out in

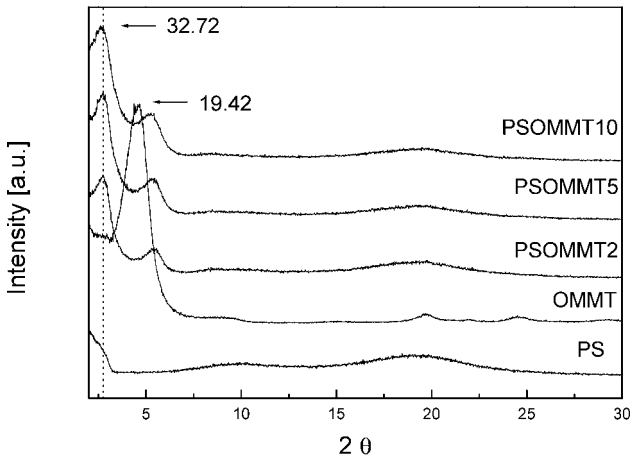

Figure 1 The XRD diffractogram of the PS, OMMT, and PS/OMMT nanocomposites.

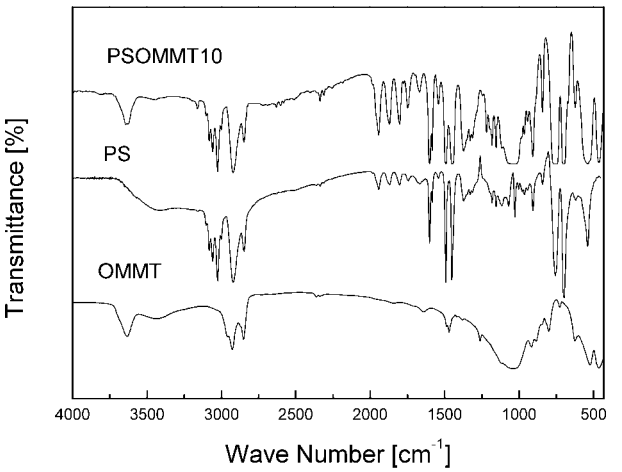

Figure 2 FTIR spectra of the PS, OMMT, and PS/OMMT nanocomposite containing 5 wt % OMMT.

the parallel plate geometry, and the complex shear modulus ($G^* = G' + iG''$, where G' is the storage modulus and G'' is the loss modulus) and complex viscosity ($\eta^* = \eta' - i\eta''$) were measured as functions of the frequency with a deformation of 0.3% at 200°C.

RESULTS AND DISCUSSION

Figure 1 presents XRD diffractograms of the PS and various representative nanocomposites. The d_{001} spacings were calculated from the Bragg formula, $d = \lambda/2 \sin \theta$, at peak positions (wavelength λ of X ray = 1.54 Å). Because of the intercalation of PS into the galleries via the solvent casting method, the d_{001} spacing of OMMT increased from 19.42 to 32.72 Å of the nanocomposite in the dry state. The PS is considered to be intercalated into the interlayer galleries because of the slight Lewis base character imparted by the phenyl ring, leading to favorable interactions with the silicate layers.[42] The d_{001} spacing for the PS/OMMT nanocomposites is independent of the clay loading, which is consistent with the model PS-based nanocomposites of Vaia and coworkers.[43,44] Even though the XRD patterns of the nanocomposites were not observed for $2\theta < 1.5°$, the XRD patterns of the overall nanocomposites are similar to that of OMMT. This is a strong indication that the overwhelming fraction of the OMMT nanocomposite retains the crystalline structure (i.e., there is no trace in the occurrence of the delamination). Consequently, the XRD analysis leads to a conclusion that the PS is intercalated into the interlayer of OMMT.

The FTIR spectrum of the representative composite is illustrated in Figure 2 along with those of PS, OMMT, and PSOMMT10. The spectrum of the nanocomposite clearly exhibits the characteristic absorptions attributable to both the polymeric organic and inorganic groups. The absorption bands at 3070 and 3030 (aromatic C—H stretching), 2960 and 2930 (aliphatic C—H stretching), and 2926 and 2852 cm^{-1} (asymmetric and symmetric vibration of —CH_2) are the frequencies of PS. The absorption bands for OMMT are 3636 (—OH stretching vibration of OMMT), 1037 (Si—O stretching vibrations of OMMT), and 522 and 466 cm^{-1} (Al—O stretching and Si—O bending vibrations of OMMT). Also, the C—H asymmetric and symmetric stretching vibration in the alkyl chains of the ammonium salt are 2929 and 2852 cm^{-1}, respectively.

Figure 3 represents the TGA thermograms of PS and PS/OMMT nanocomposites with various OMMT contents. In contrast to the PS, the onset of decomposition for PS/OMMT nanocomposites is shifted toward a higher temperature with the clay content. This enhancement of the thermal stability can be regarded as additional evidence of the intercalations between PS and OMMT. The OMMT possesses high thermal stability, and its layer structure exhibits a great barrier

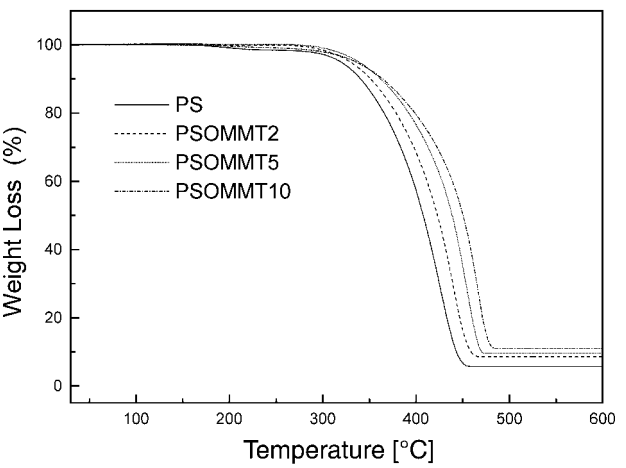

Figure 3 TGA thermograms of PS and PS/OMMT nanocomposites.

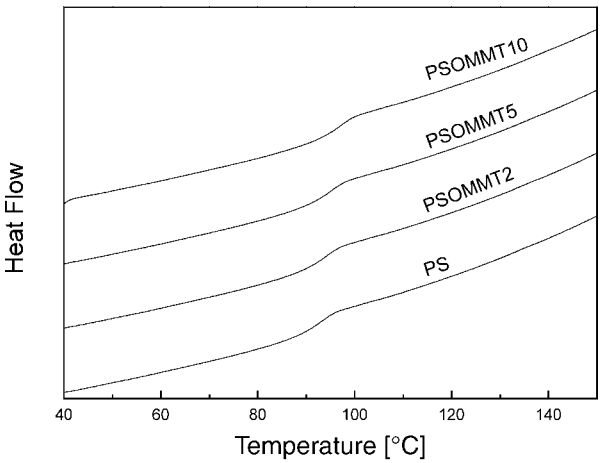

Figure 4 DSC thermograms of PS and PS/OMMT nanocomposites.

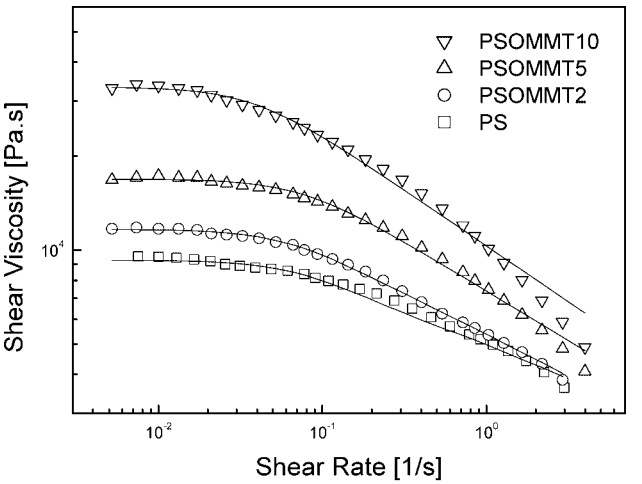

Figure 5 The steady shear viscosity versus the shear rate for PS/OMMT nanocomposites with three different clay contents at 200°C.

effect that stops the evaporation of the small molecules generated in the thermal decomposition process and effectively limits the continuous decomposition of the PS.[45,46] Also, note that the nanocomposites show approximately the same decomposition temperature at 320°C, regardless of polymer loading. This means that the thermal insulation effect of OMMT has little dependence on the contents of intercalated polymer in the concentration range we studied.[47]

The glass-transition behaviors of the PS and PS/OMMT nanocomposites measured by the DSC analysis are shown in Figure 4. The PS exhibits an endothermic peak at 94°C. When compared to the glass-transition temperature (T_g) of pure PS, the T_g of the PS/OMMT nanocomposites is linearly increased with the amount of OMMT. This is caused by the strong intercalation between PS and OMMT, which limits the cooperative dynamics of the PS main chain segments.[48]

The steady shear response of polymer/clay nanocomposites has important consequences for the processability of the materials. We have systematically studied the PS/OMMT nanocomposites via a steady shear measurement in their melt state. Figure 5 shows the steady shear viscosity (η) versus the shear rate ($\dot{\gamma}$) for the PS and PS/OMMT nanocomposites with different clay loadings at 200°C. At low shear rates, the η increases substantially and monotonically at a given $\dot{\gamma}$ with the OMMT content. However, at high shear rates, the viscosity and degree of shear thinning for the PS/OMMT nanocomposites are comparable with those of the unfilled polymer as a result of the preferential orientation of the layers of the silicates or even anisotropic tactoids parallel to the flow direction.[38,49,50] A similar trend in the shear viscosity was also observed by Krishnamoorti et al.[51] for a series of intercalated poly(dimethyl diphenyl siloxane)/silicate nanocomposites. They found not only that the shear viscosity of the nanocomposites increases monotonically with silicate loading but also that the intercalated nanocomposites display shear thinning behavior at lower shear rates, which is possibly due to the changes in orientation of the silicate layers and polymer conformation under the shear.[52]

In order to investigate the η versus $\dot{\gamma}$ relationship, we fit the measured viscosity to the Carreau model[53] given by eq. (1):

$$\eta = \frac{\eta_0}{[1 + (\lambda_c \dot{\gamma})^2]^{(1-n)/2}} \tag{1}$$

Here η_0 is the zero shear rate viscosity, λ_c is a characteristic (or relaxation) time, and n is a dimensionless parameter, where the slope of η versus $\dot{\gamma}$ in the power-law region is given by $(n - 1)$. Note that in the special case of $n = 1$ or $\dot{\gamma}\lambda_c \to 0$, eq. (1) reduces to the Newtonian fluid model. For $n < 1$, eq. (1) predicts shear thinning behavior. From the calculated values for parameters n, λ_c, and η_0 in the PS/OMMT nanocomposites system (Table I), we found that the degree of shear thinning and λ_c increase with the OMMT content. The degree of shear thinning increases with clay loading (Fig. 5) because of the alignment of the clay layer structures under the shear,[51,54] meaning that the suspension microstructure changes from a random

TABLE I
Carreau Model [Eq. (1)] Parameters Obtained from PS and PS/OMMT Nanocomposite Systems

Sample Codes	η_0 (Pas) $\times 10^{-4}$	λ_c (s)	n
PS	0.93	12.53	0.77
PSOMMT2	1.17	14.54	0.72
PSOMMT5	1.69	13.34	0.68
PSOMMT2	3.33	26.26	0.64

orientation to a shear-induced orientation.[35] Note that the shear thinning viscosities of biodegradable aliphatic polyester (BAP)/poly(vinyl alcohol) blends[55] and poly(ethylene oxide)/clay nanocomposites[35] also fit the Carreau model quite well.

The dynamic linear viscoelastic behavior of the nanocomposites in a melt state is examined in a constant strain rheometer in either a cone–plate or parallel plate geometry. The linearity in the measurements is typically confirmed by repeating the measurements at higher and lower strain amplitudes and observing the independence of the measured G' and G'' values. For the nanocomposites with low clay loading a linear viscoelasticity is observed for strain amplitudes below 5%, while for the higher clay nanocomposites a linear viscoelastic response is observed over a more restricted strain amplitude range. Nonlinear effects are being observed in some cases for strain amplitude as small as 1%.[56] In our experiment the linear viscoelasticity for the nanocomposites was observed only for a limited range of strain (0.3%). The G' and G'' values for the PS/OMMT nanocomposites as functions of the angular frequency (ω) with various clay contents are shown in Figure 6. The G' and G'' values of these nanocomposites show a monotonic increase at all frequencies with OMMT loading. The slope of G' and G'' in the terminal zone was estimated for all four samples at a frequency below 2 1/s. The frequency dependence of G' decreases monotonically (i.e., the transition from ω to $\omega^{0.94}$ for PS, to $\omega^{0.94}$ for PSOMMT2, to $\omega^{0.84}$ for PSOMMT5, and to $\omega^{0.62}$ for PSOMMT10). Also, the frequency dependence of G'' is altered with clay loading (i.e., $\omega^{0.66}$ for PS, $\omega^{0.62}$ for PSOMMT2, $\omega^{0.57}$ for PSOMMT5, and $\omega^{0.46}$ for PSOMMT10). Similar trends in the oscillatory shear experiment were also observed by Krishnamoorti and Gianellis[56] for a series of nylon 6/MMT and poly(ϵ-caprolactone)/MMT nanocomposites for the polymer chains being end tethered to the silicate surface via a cationic surfactant. The slope and absolute values of the dynamic moduli indicate a supermolecular structure formation in the nanocomposites. The higher the G' and the smaller the slope, the more pronounced the interaction between the silicate sheets and their tendency to form a 3-dimensional superstructure.[57] Rheological measurements performed on PS-based model nanocomposites have shown that the formation of a superstructure results in a well-pronounced equilibrium plateau modulus.[29]

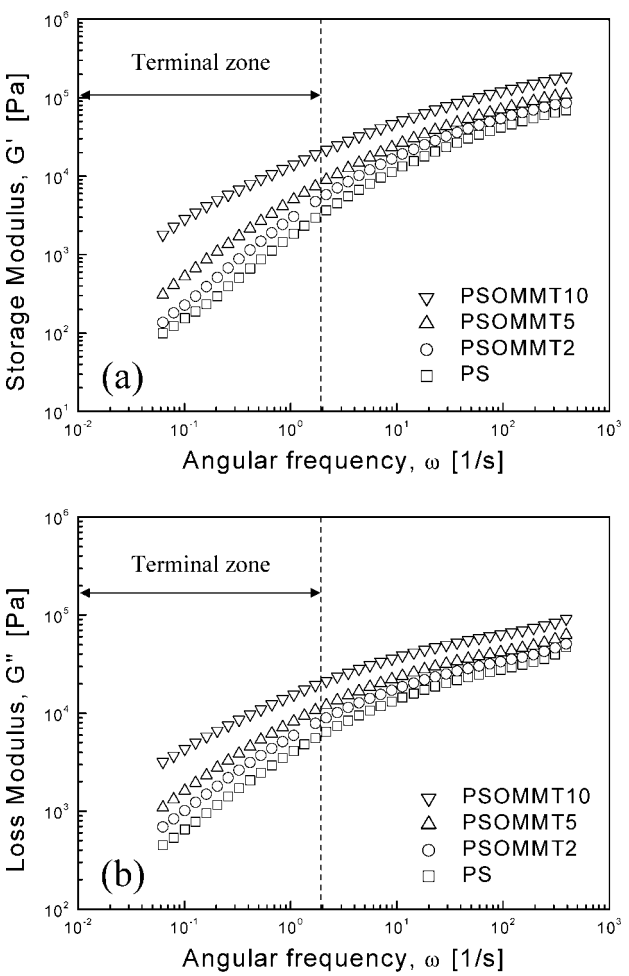

Figure 6 The linear viscoelastic dynamic moduli (a) G' and (b) G'' for PS/OMMT nanocomposites at 200°C.

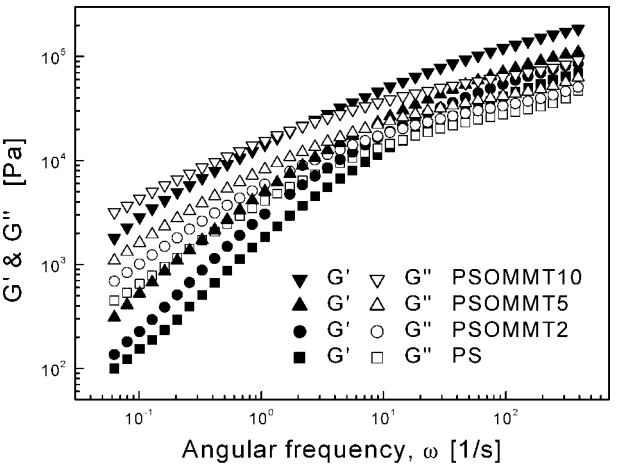

Figure 7 The values for G' and G'' as a function of ω for PS and PS/OMMT nanocomposites.

Larson[58] illustrated G' and G'' values for prototypical solidlike and liquidlike materials. The G' and G'' versus ω values for nanocomposites are shown in Figure 7. For $G' < G''$, we expect liquidlike behavior; for $G' > G''$ and G' is nearly independent of the frequency, we expect solidlike behavior. The melt behavior of the PS is liquidlike ($G' < G''$) at low frequencies, while solidlike behavior is found at high frequencies ($G' > G''$). In the case of PS, the transition from liquidlike to solidlike occurs at $\omega_c \sim 14$ 1/s, as indicated by the crossover of G' and G'' values. In contrast to PS, the crossover point for PS/OMMT nanocom-

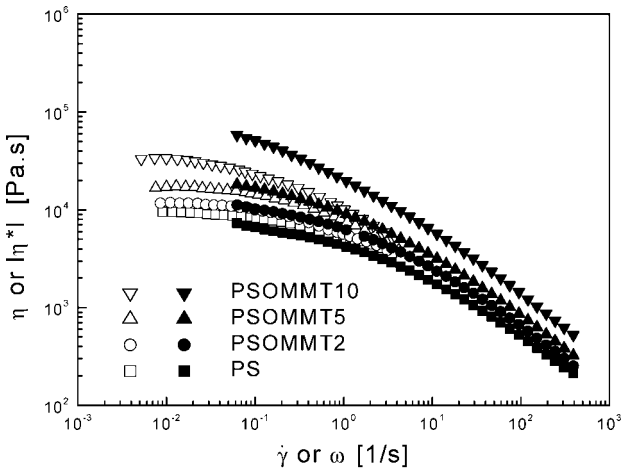

Figure 8 The values for (open symbols) η versus $\dot{\gamma}$ and (filled symbols) $|\eta^*|$ versus ω for PS and PS/OMMT nanocomposites at 200°C.

posites is shifted toward a lower angular frequency with the clay content.

For highly elastic fluids and polymer melts, it is very difficult to measure the steady shear viscosity at high shear rates. The shear viscosity can be estimated from the Cox–Merz relation. Figure 8 shows that the shear viscosity of the PS/OMMT nanocomposites was obtained via steady shear experiments and η^* was obtained from the oscillatory experiments as a function of $\dot{\gamma}$ and ω. Cox and Merz[59] found that the modulus of the complex viscosity $[\eta^* = G^*/(i\omega)]$ was roughly equal to the viscosity obtained at $\dot{\gamma} = \omega$. The empirical Cox–Merz relation is

$$\eta(\dot{\gamma}) = |\eta^*(\omega)|_{\dot{\gamma}=\omega} = \sqrt{(\eta')^2 + (\eta'')^2} \qquad (2)$$

This is important because it allows us to determine the shear rate dependence of the viscosity at shear rates significantly higher than those permitted for cone–plate and plate–plate geometries.[60] Both the η and $|\eta^*|$ of the PS/OMMT nanocomposites decrease with increasing $\dot{\gamma}$ or ω and increase with increasing clay content. The $|\eta^*|$ fit η at low clay content but deviate at high clay loading. The mechanism for this deviation is possibly attributable to orientation of the silicate layers. Note that oscillatory shear, when applied in the linear viscoelastic region, may be able to promote the shear thinning capability of materials. By contrast, steady shear can effectively rearrange molecular packing of materials along the shear direction. Lin and Winter[61] reported that the η value of liquid crystalline polymers is much lower than their $|\eta^*|$ value due to the better molecular alignment achieved by steady shear. Thus, the Cox–Merz relation for the PS/OMMT nanocomposites is invalid for high frequency and/or high clay content.

CONCLUSIONS

We prepared PS/OMMT nanocomposites via a solvent casting method using chloroform as the cosolvent. The XRD analysis and FTIR spectra confirmed the insertion of PS between the layers of the OMMT. The TGA and DSC analyses showed that the thermal stability of PS/OMMT nanocomposites becomes higher than PS as the OMMT content increases. From the rheological measurement, an η increase was observed as the OMMT loading increased. The PS/OMMT nanocomposites exhibit higher zero shear rate viscosity and pronounced shear thinning behavior. Also, the G' and G'' values of PS/OMMT nanocomposites showed a monotonic increase with OMMT loading at all frequencies. The slope of G' and G'' in the terminal zone decreases sharply at frequencies below 2 1/s, and the crossover points of G' and G'' for PS/OMMT nanocomposites are shifted toward a lower ω with increasing clay content. This phenomenon results in a shift from liquidlike to solidlike behavior. Finally, the Cox–Merz relation for the PS/OMMT nanocomposites is invalid for high frequency and/or high clay content.

The authors acknowledge support for this study by research grants from the Korea Science and Engineering Foundation (KOSEF) through the Applied Rheology Center (ARC), an official KOSEF-created engineering research center at Korea University, Seoul.

References

1. Strawhecker, K. E.; Manias, E. Chem Mater 2000, 12, 2943.
2. Yano, K.; Usuki, A. J Polym Sci Part A Polym Chem 1997, 35, 2289.
3. Petrović, Z. S.; Javni, I.; Waddon, A.; Bánhegyi, G. J Appl Polym Sci 2000, 76, 133.
4. Ryu, J. G.; Lee, P. S.; Kim, H.; Lee, J. W. Kor Austral Rheol J 2001, 13, 61.
5. Liu, X.; Wu, Q.; Berglund, L. A.; Fan, J.; Qi, Z. Polymer 2001, 42, 8235.
6. Rong, J.; Jing, Z.; Li, H.; Sheng, M. Macromol Rapid Commun 2001, 22, 329.
7. Alexandre, M.; Beyer, G.; Henrist, C.; Cloots, R.; Rulmont, A.; Jérome, R.; Dubois, P. Macromol Rapid Commun 2001, 22, 643.
8. Yong ,Y.; Zhn, Z.; Yin, J.; Wang, X.; Qi, Z. Polymer 1999, 40, 4407.
9. Gläsel, H. J.; Bauer, F.; Ernst, H.; Findeisen, M.; Hartmann, E.; Langguth, H.; Mehnert, R.; Schubert, R. Macromol Chem Phys 2000, 201, 2765.
10. Burnside, S. D.; Giannelis, E. P. Chem Mater 1995, 7, 1597.
11. Kim, B. H.; Jung, J. H.; Kim, J. W.; Choi, H. J.; Joo, J. Synth Met 2001, 121, 1311.
12. Vaia, R. A.; Vasudevan, S.; Krawieew, W.; Scanlon, L. G.; Giannelis, E. P. Adv Mater 1995, 7, 154.
13. Kim, B. H.; Jung, J. H.; Kim, J. W.; Choi, H. J.; Joo, J. Synth Met 2001, 117, 115.
14. Kim, B. H.; Jung, J. H.; Joo, J.; Epstein, A. J.; Mizoguchi, K.; Kim, J. W.; Choi, H. J. Macromolecules 2002, 35, 1419.
15. Yeh, J. M.; Liou, S. J.; Lai, C. Y.; Wu, P. C.; Tsai, T. Y. Chem Mater 2001, 13, 1131.

16. Lee, D.; Lee, S. H.; Char, K.; Kim, J. Macromol Rapid Commun 2000, 21, 1136.
17. Kim, J. W.; Kim, S. G.; Choi, H. J.; Jhon, M. S. Macromol Rapid Commun 1999, 20, 450.
18. Choi, H. J.; Kim, J. W.; Noh, M. H.; Lee, D. C.; Suh, M. S.; Shin, M. J.; Jhon, M. S. J Mater Sci Lett 1999, 18, 1505.
19. Choi, H. J.; Kim, J. W.; Joo, J.; Kim, B. H. Synth Met 2001, 121, 1325.
20. Kim, J. W.; Noh, M. H.; Choi, H. J.; Lee, D. C. Jhon, M. S. Polymer 2000, 41, 1229.
21. Park, J. H.; Park, O. O. Kor Austral Rheol J 2001, 13, 61.
22. Choi, H. J.; Cho, M. S.; Kim, J. W.; Kim, C. A.; Jhon, M. S. Appl Phys Lett 2001, 78, 3806.
23. Sim, I. S.; Kim, J. W.; Choi, H. J.; Kim, C. A.; Jhon, M. S. Chem Mater 2001, 13, 1243.
24. Huang, J. C.; Zhu, Z. K.; Yin, J.; Qian, X. F.; Sun Y. Y. Polymer 2001, 42, 873.
25. Vaia, R. A.; Giannelis, E. P. Macromolecules 1997, 30, 8000.
26. Balazs, A. C.; Singh, C.; Zhulina, E.; Lyatskaya, Y. Acc Chem Res 1999, 32, 651.
27. Friedlander, H. Z.; Grink, C. R. J Polym Sci Polym Lett 1964, 2, 475.
28. Mohan, S.; Laura, N.; Cerini, S. S.; Ghosh, K. I. W. J Polym Sci Part B Polym Phys 1996, 34, 1443.
29. Hoffmann, B.; Dietrich, C.; Thomann, R.; Friedrich, C.; M̈lhaupt, R. Macromol Rapid Commun 2000, 21, 57.
30. Noh, M. W.; Lee, D. C. Polym Bull 1999, 42, 619.
31. Chen, G.; Liu, S. S.; Chen, S.; Qi, Z. Macromol Chem Phys 2001, 202, 1189.
32. Ogata, N.; Jiménez, G.; Kawai, H.; Ogihara, T. J Polym Sci Part B Polym Phys 1997, 35, 389.
33. Jiménez, G.; Ogata, N.; Kawai, H.; Ogihara, T. J Appl Polym Sci 1997, 64, 2211.
34. Ogata, N.; Kawakage, S.; Ogihara, T. J Appl Polym Sci 1997, 66, 573.
35. Choi, H. J.; Kim, S. G.; Hyun, Y. H.; Jhon, M. S. Macromol Rapid Commun 2001, 22, 320.
36. Jordan, J. W. J Phys Colloid Chem 1949, 53, 294.
37. Kwon, O. Y.; Park, K. W. J Ind Eng Chem 2001, 7, 44.
38. Pinnavaia, T. J.; Beall, G. W. Polymer–Clay Nanocomposites; Wiley: Chichester, U.K., 2000.
39. LeBaron, P. C.; Pinnavaia, T. J. Chem Mater 2001, 13, 3760.
40. Zilg, C.; Thomann, R.; Baumert, M.; Finter, J.; Mülhaupt, R. Marcromol Rapid Commun 2000, 21, 1214.
41. Xie, W.; Gao, Z.; Liu, K.; Pan, W. P.; Vaia, R.; Hunter, D.; Singh, A. Thermochim Acta 2001, 340, 367.
42. Hackett, E.; Manias, E.; Giannelis, E. P. J Chem Phys 1998, 108, 7410.
43. Vaia, R. A.; Giannelis, E. P. Macromolecules 1997, 30, 7990.
44. Vaia, R. A.; Jandt, K. D.; Kramer, E. J.; Giannelis, E. P. Macromolecules 1995, 28, 8080.
45. Burnside, S. D.; Giannelis, E. P. Chem Mater 1995, 7, 1597.
46. Yano, K.; Usuki, A.; Kurauchi, T.; Kamigato, O. J Polym Sci Part A Polym Chem 1993, 31, 2493.
47. Noh, M. H.; Jang, L. W.; Lee, D. C. J Appl Polym Sci 1999, 74, 183.
48. Huang, J. C.; Zhu, Z.; Yin, J.; Qian, X.; Sun, Y. Y. Polymer 2001, 42, 877.
49. Lim, S. T.; Hyun, Y. H.; Choi, H. J.; Jhon, M. S. Chem Mater 2002, 14, 1839.
50. Kim, T. H.; Jang, L. W.; Lee, D. C.; Choi, H. J.; Jhon, M. S.; Macromol Rapid Commun 2002, 23, 191.
51. Krishnamoorti, R.; Vaia, R. A.; Giannelis, E. P. Chem Mater 1996, 8, 1728.
52. Manias, E.; Hadziioannou, G.; Brinke, G. T. Langmuir 1996, 12, 4587.
53. Carreau, P. J.; De Kee, D. C.; Chhabra, R. P. Rheology of Polymeric Systems: Principles and Application; Hanser: New York, 1997.
54. Hyun, Y. H.; Lim, S. T.; Choi, H. J.; Jhon, M. S. Macromolecules 2001, 34, 8084.
55. Shin, T. K.; Kim, J.; Choi, H. J.; Jhon, M. S. J Appl Polym Sci 2000, 77, 1348.
56. Krishnamoorti, R.; Giannelis, E. P. Macromolecules 1997, 30, 4097.
57. Hoffmann, B.; Kressler, J.; Stöppelmann, G.; Friedich, Chr.; Kim, G. M. Colloid Polym Sci 2000, 278, 629.
58. Larson, R. G. The Structure and Rheology of Complex Fluids; Oxford University Press: New York, 1999.
59. Cox, W. P.; Merz, E. H. J Polym Sci 1958, 28, 619.
60. Riande, E.; Diaz-Calleja, R.; Prolongo, M. G.; Masegosa, R. M.; Salom, C. Polymer Viscoelasticity; Marcel Dekker: New York, 2000.
61. Lin, Y. G.; Winter, H. H. Polym Eng Sci 1992, 37, 773.